

# Intrinsic Spin Photogalvanic Effect in Nonmagnetic Insulator

Ruixiang Fei,<sup>1</sup> Xiaobo Lu,<sup>1</sup> and Li Yang<sup>1,2</sup>

<sup>1</sup>*Department of Physics, Washington University in St Louis, St Louis, Missouri 63130, United States*

<sup>2</sup>*Institute of Materials Science and Engineering, Washington University in St. Louis, St. Louis, Missouri 63130, United States*

We show that with the help of spin-orbit coupling, nonlinear light-matter interactions can efficiently couple with spin and valley degrees of freedom. This unrevealed spin photogalvanic effect can drive the long-time pursued intrinsic pure spin current (PSC) in noncentrosymmetric, nonmagnetic insulators. Different from the spin and valley Hall effect, such a photo-driven spin current is universal and can be generated without bias. Using first-principles simulation, we take monolayer transition metal dichalcogenides (TMDs) to demonstrate this effect and confirm an enhanced PSC under linear polarization. The amplitude of PSC is one order larger than the observed charge current in monolayer TMDs. This exotic nonlinear light-spin interaction indicates that light can be utilized as a rapid fashion to manipulate spin-polarized current, which is crucial for future low-dissipation nanodevice.

**Introduction.**– Spintronics is promising for developing the next generation of energy-efficient electronics because it reduces Joule heating and Oersted fields while retains the functionality of spin currents to manipulate magnetization [1–4]. Pure spin current (PSC), in which electrons with different spins travel in opposite directions and there is no net motion of charge [5], is highly desired for spintronic devices[6, 7]. To date, the generation of PSC in a rapid and controllable manner represents a challenging research direction [8]. PSC has been induced by the means of spin pumping [9–12], spin Seebeck[13–15], spin Nernst effect[16, 17], and the spin Hall effect [18–22]. Nevertheless, for spin pumping, spin Seebeck or spin Nernst, it is difficult to realize well-localized microwave and terahertz fields or temperature gradients at the nanoscale in a rapid fashion. Alternatively, the spin Hall effect can converts a longitudinal charge current to a transverse PSC via extrinsic spin-dependent Mott scatterings [18, 19] or the spin-orbit coupling (SOC) [23–25]. However, a charge current is required, and Joule heating is not fundamentally avoided.

Light-matter interactions is a fundamental topic of condensed matter physics. Light has been utilized as a powerful tool to rapidly and precisely manipulate a wide range of properties. Particularly, the spin-polarized current accompanied by a net charge current[26, 27] or the PSC [28, 29] was observed by applying circularly polarized radiation on quantum interference systems, e.g. quantum wells. More recently, the photo-induced PSC was observed in a heterostructure composed of a platinum layer and a yttrium-iron garnet (YIG) film [30]. However, all the above spin currents were generated in complex quantum systems and require extrinsic mechanisms, such as interface engineering and the proximity effect. For example, the photo-spin current in platinum is originated from the magnetic insulator YIG [30], which is not an intrinsic effect of a single crystal. Therefore, finding a fundamentally new and intrinsic mechanism of light-spin interactions is essential to overcome these challenges.

Second-order nonlinear optical (NLO) responses have been known to be able to create DC current or photovoltage in noncentrosymmetric semiconductors. For example, shift current is the microscopic mechanism of the linear bulk photovoltaic (BPV) effect[31–33], while injection current is the origin of the circular photogalvanic effect [33–35] in time-reversal invariant materials. Nevertheless, those studies have focused on charge currents. How light interacts with spins of electrons is mostly unknown, and corresponding theoretical framework have yet established. In this work, we find that spins and valleys of electrons can strongly couple with light via second-order optical responses in noncentrosymmetric materials. This mechanism can selectively generate PSC or spin polarized current in nonmagnetic materials, which we called it the intrinsic spin photogalvanic effect.

**Theory and Mechanism.**– We consider time-reversal invariant noncentrosymmetric semiconductors with sizable SOC. We use monolayer transition metal dichalcogenides (TMDs) to demonstrate our theory. The typical band structures around band edges are shown in Figs. 1a and 1b. The spin-up and spin-down bands at  $K/-K$  points of reciprocal space are split by SOC and the spin order is reversed due to time-reversal symmetry. Under coherent light illumination, the second-order nonlinear DC photocurrent density is

$$J_c = \chi_{abc}(0; \omega, -\omega) E_a(\omega) E_b(-\omega) \quad (1)$$

where  $E(\omega)$  is the electrical field of incident light with a frequency  $\omega$ , indices  $a$  and  $b$  are the light polarization directions, and  $c$  is the current direction. The  $\chi_{abc}(0; \omega, -\omega)$  is the second-order current susceptibility, which has contributions from interband excitation, so-called shift current and injection current, and intraband nonlinear process, namely the optical rectification or the nonlinear Hall conductivity [36–41]. For semiconductors, the intraband nonlinear process can be neglected because of the Berry-curvature dipole ( $\partial_k \Omega^c$ ) is zero at the chemical potential located within the bandgap. Thus, we focus on the leading-order interband contribu-

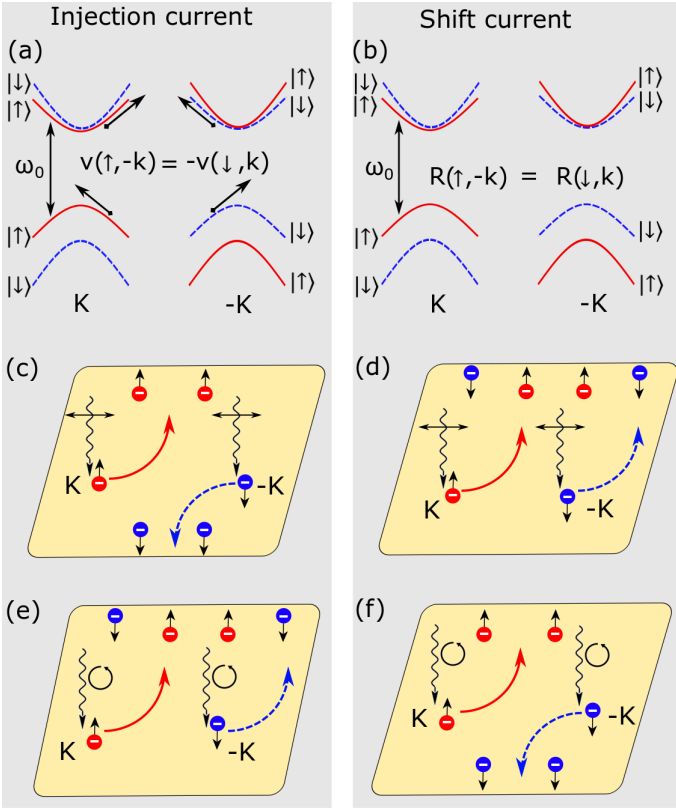


FIG. 1. Mechanisms of the spin photogalvanic effect: (a) Injection-current mechanism of monolayer TMDs. It is decided by the group velocity, which is odd in reciprocal space. (b) Shift-current mechanism of monolayer TMDs. It is decided by the shift vector, which is even in reciprocal space. (c) PSC generated by the injection-current mechanism under linearly polarized light. (d) Charge current generated by the shift-current mechanism under linearly polarized light. (e) Charge current generated by the injection-current mechanism under circularly polarized light. (f) PSC generated by the shift-current mechanism under circularly polarized light.

tions in the following, i.e., the shift-current mechanism ( $\chi_{abc}(0; \omega, -\omega) \equiv \sigma_{abc}(0; \omega, -\omega)$ ) and injection-current mechanism ( $\chi_{abc}(0; \omega, -\omega) \equiv \eta_{abc}(0; \omega, -\omega)$ ).

*Photocurrents under Linearly polarization:* Using quantum perturbation theory, the DC photoconductivity of injection current is (see Supplementary Section I [42] and refs.[33, 43])

$$\eta_{abc}^L = \frac{-\pi e^3}{\hbar^2 \omega^2} \sum_{mn} \int d^3 k \alpha_{mn}^{ab}(k) (v_{mm}^c(k) - v_{nn}^c(k)) \cdot \tau \delta(\omega - \omega_{mn}) \quad (2)$$

where  $\alpha_{mn}^{ab}(k) = \frac{1}{2}(v_{mn}^a(k)v_{nm}^b(k) + v_{mn}^b(k)v_{nm}^a(k))$  is the optical oscillate strength.  $v_{mn}^a(k)$  and  $v_{nm}^b(k)$  are the  $a$ -direction and  $b$ -direction velocity matrices between the conduction band  $m$  and the valence band  $n$ , respectively.  $v_{mm}^c(k)$  is the  $c$ -direction intraband velocity matrix.  $\tau$

is the relaxation time of free carriers. In time-reversal invariant materials, the optical oscillate strength  $\alpha_{mn}^{ab}(k)$  is even, while the term  $v_{mm}^c(k) - v_{nn}^c(k)$  describing the group-velocity difference between electrons and holes is odd in reciprocal space, as schematically plotted in Fig. 1a. As a result, Eq. 2 indicates that the overall injection-current photo-conductivity is odd. Given the opposite orders of spin-up and spin-down bands between  $K$  and  $-K$  valleys, if pumped by photons ( $\omega_0$ ), the current direction of spin-up electrons at the  $K$  valley is opposite to that of spin-down electrons at the  $-K$  valley (Fig. 1c). Namely, linearly polarized light excites two different spins to travel in opposite directions, resulting in a PSC.

Then we turn to the discussion of shift current in the form of (see Supplementary section IIA [42])

$$\sigma_{abc}^L = \frac{\pi e^3}{\hbar^2 \omega^2} \sum_{mn} \int d^3 k \alpha_{mn}^{ab}(k) R_{nm}^c \delta(\omega - \omega_{mn}) \quad (3)$$

where the so-called shift vector  $R_{nm}^c = \frac{\partial \phi_{nm}^b}{\partial k_c} - (A_{nn}^c(k) - A_{mm}^c(k))$  is the difference between Berry connections of the conduction band ( $A_{mm}^c(k)$ ) and the valence band ( $A_{nn}^c(k)$ ).  $\phi_{nm}^b$  is the phase of the interband velocity matrix  $v_{nm}^b(k)$ . Because of time-reversal symmetry, the shift vector and its photoconductivity are even in reciprocal space, as plotted in Fig. 1(b). Thus, for incident photons at the frequency  $\omega_0$ , the direction of spin-up current from the  $K$  valley is the same as that of spin-down current from the  $-K$  valley. As concluded in Fig. 1d, two different spin electrons travel in the same direction, forming a non-spin-polarized charge current. This is the linearly photogalvanic effect or linearly bulk photovoltaic effect.

*Photocurrents under circular polarization:* The circularly-polarized photoconductivity of injection current is

$$\eta_{abc}^{\circ} = \frac{2\pi i e^3}{\hbar^2 \omega^2} \sum_{mn} \int d^3 k \text{Im}(v_{mn}^a(k)v_{nm}^b(k)) \cdot (v_{mm}^c(k) - v_{nn}^c(k)) \tau \delta(\omega - \omega_{mn}) \quad (4)$$

Recalling the Kubo formula of Berry curvature,  $\Omega^c(k) = \frac{\text{Im}(v_{mn}^a(k)v_{nm}^b(k))}{E_{mn}^2}$  [44], the parity of  $\text{Im}(v_{mn}^a(k)v_{nm}^b(k))$  is the same as that of Berry curvature, which is odd in reciprocal space under time-reversal symmetry [25]. Given that the intraband transition matrices ( $v_{mm}^c(k)$  and  $v_{nn}^c(k)$  in Eq. 4) are odd, the overall circularly-polarized photoconductivity is even in reciprocal space. This indicates that spin-up and spin-down electrons travel in the same direction, forming a non-spin-polarized charge current as shown in Fig. 1e. This so-called circularly photogalvanic effect has been observed in monolayer WSe<sub>2</sub> [45].

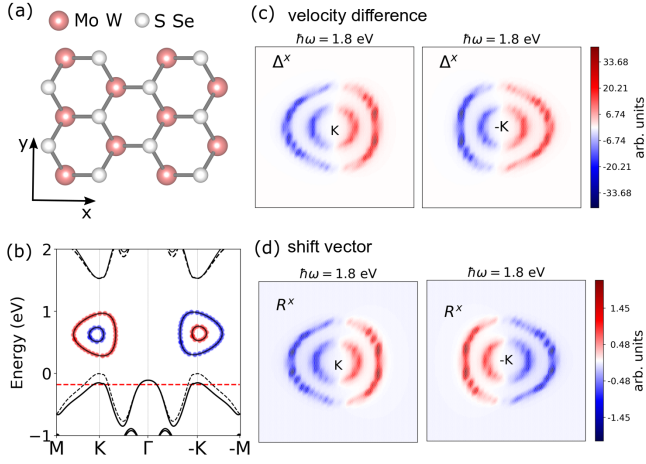


FIG. 2. First-principles calculated results: (a) Top view of the structure of monolayer group-VI dichalcogenides. (b) Bandstructure of monolayer MoS<sub>2</sub>. The inset is the calculated spin texture of electronic states crossed by the red dashed line. Blue and red dots represent the spin up and down along the  $z$ -direction, respectively. (c) Group velocity difference for  $\hbar\omega = 1.8$  eV photon excitation. (d) Shift vector for  $\hbar\omega = 1.8$  eV photon excitation.

Finally, the circularly-polarized photoconductivity of shift current is

$$\sigma_{abc}^{\odot} = \frac{-2i\pi e^3}{\hbar^2\omega^2} \sum_{mn} \int d^3k \operatorname{Im}(v_{mn}^a(k)v_{nm}^b(k)) \cdot R_{nm}^c(k)\delta(\omega - \omega_{mn}) \quad (5)$$

Due to the odd parity of  $\operatorname{Im}(v_{mn}^a(k)v_{nm}^b(k))$  and even parity of shift vector  $R_{nm}^c(k)$  in reciprocal space, the overall photoconductivity is odd. Thus, the light-excited spin-up and spin-down electrons transport in the opposite direction, forming a PSC as schematized in Fig. 1f. This unrevealed spin-polarized current may be one of the mechanisms responding for photo-induced spin current observed in quantum well systems [28, 29].

#### Spin and charge currents in monolayer TMDs.

The observed spin polarization depends on the competition between the above-discussed currents in specific materials. In the following, we choose monolayer TMDs (Fig. 2a) as a prototypical family of materials for first-principles simulations (see details in Supplementary Section III [42, 46–49]). The SOC and broken inversion symmetry enable the valley-spin locking in monolayer structures and induce the known spin and valley Hall effects [25] and circular dichroism [50–52]. In Fig. 2b, we show the first-principles calculated band structure of monolayer MoS<sub>2</sub>. The SOC splitting of the top two valence bands is around 150 meV at  $K/-K$  points, which is similar to previous work [53]. The inset plot shows the spin texture of electronic states around the  $K$  and  $-K$  points below the top of valence bands (marked by a horizontal dashed line). It is interesting but not surprising to find

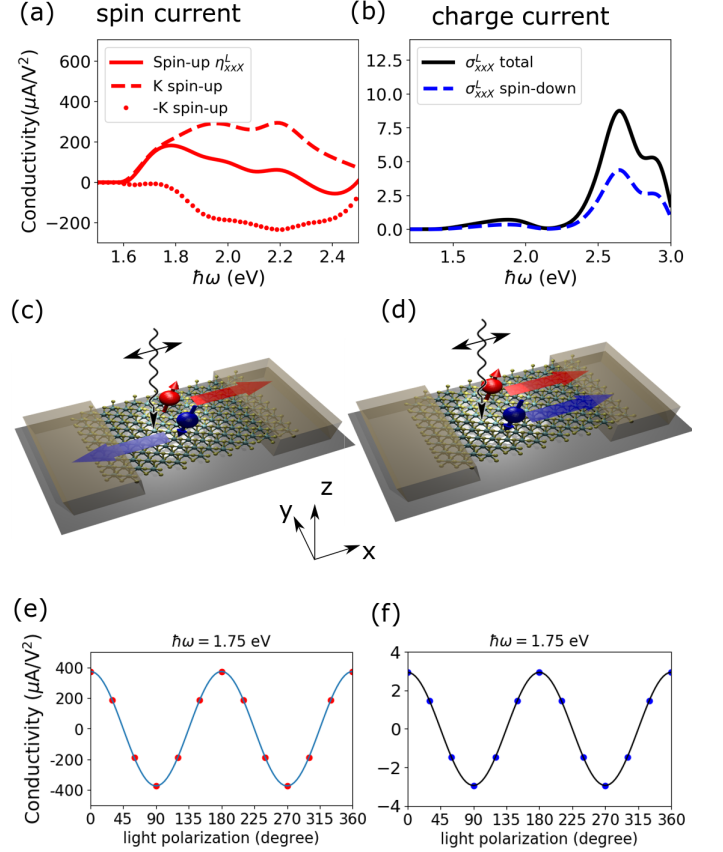


FIG. 3. PSC under linear polarization: (a) Calculated  $x$ -direction spin-up current conductivity  $\eta_{xxx}^L$  in monolayer MoS<sub>2</sub>. (b) Charge current conductivity  $\sigma_{xxx}^L$  along the  $x$ -direction. The  $x$ -direction defined in Fig. 2 (a). The schematic plots of light-induced the PSC (c) and charge current (d). (e) and (f) The light polarization direction-dependent spin current and charge current for  $\hbar\omega = 1.75$  eV photon excitation, respectively. The zero-degree is set to be along the  $x$ -direction.

that nearly all spins are along the  $z$ -axis, that is  $\sigma_z = \pm 1$ , for electrons around  $K$  and  $-K$  points [54].

As determined by Eqs. 2-5, the origins of spin and charge currents are mainly from parities of the group velocity difference  $\Delta_{mn}^c = v_{mm}^c(k) - v_{nn}^c(k)$  and shift vector  $R_{nm}^c(k)$ , respectively. Figs. 2c and 2d show these physical quantities for the photon energy  $\hbar\omega = 1.8$  eV, which pumps electrons around  $K$  and  $-K$  points. For the sake of simplicity, only  $x$  components of these quantities are plotted. It is clear to see that the group velocity difference is even while the shift vector is odd according to the  $\Gamma$  point of reciprocal space. This agrees with our aforementioned discussion.

*Linear-polarization induced PSC:* We employ the first-principles simulation [42] to calculate photocurrents and photo-induced spin current. First, we focus on the injection current. For monolayer TMDs showed in Fig. 2 (a), only the  $x$ -direction inject current is nonzero while the

$y$ -direction current is zero because of the mirror symmetry with respect to the  $x$ -axis. According to Eq. 2, the carrier relaxation time  $\tau$  is needed for obtaining quantitative results. Previous studies show that this relaxation time is substantially smaller than the observed spin-relaxation time and electron-hole recombination time [55–57]. Therefore, we conservatively choose  $\tau = 0.2$  ps based on results of monolayer MoS<sub>2</sub> at 300 K [58, 59], which is significantly smaller than the estimated spin-relaxation time  $\tau = 40$  ps at room temperature [60, 61].

Fig. 3a shows the calculated spectrum of spin-up-current conductivity excited by light polarized along the  $x$ -direction. The dashed red line is the contribution from the  $K$  valley, and the dotted red line is that from the  $-K$  valley. The  $K$ -valley contribution is positive (along the  $x$ -direction) and starts from the DFT bandgap at 1.6 eV while the  $-K$  valley contribution is negative and starts from 1.75 eV because of the 150 meV SOC splitting (Figure 2 (b)). Because of this competition, the total spin-up current (solid red line) is along the  $x$ -direction and reaches the maximum value at 1.75 eV. Meanwhile, the light will also excite the spin-down current dominated by band edges at the  $-K$  point but along the opposite ( $-x$ ) direction, and the total spin-down current has the same amplitude as the spin-up current. As a result, spin-up and spin-down currents are in opposite direction and result in a zero-charge current, forming a PSC by linearly polarized light shown in Fig. 3c.

The linearly-polarized light will also generate shift current, and its spectrum is presented in Fig. 3b. Importantly, both spin-up and spin-down carriers contributed equally to the total current along the same direction, as schematically shown in Fig. 3d. This agrees with the discussion of Eq. 3. The total current is a charge current but not spin-polarized. However, the spin current amplitude in Fig. 3a is about two orders of magnitude larger than that of the charge current in Fig. 3b. Therefore, the spin-polarized inject current will dominate observed photocurrent of monolayer MoS<sub>2</sub> under linearly polarized light, and a nearly 100% PSC is expected.

We also calculate the spin current of the other important monolayer TMDs, e. g., MoSe<sub>2</sub>, WS<sub>2</sub>, and WSe<sub>2</sub>. Table I summarizes the characteristic photoconductivity caused by two mechanisms at photon energy that starts to pump the second spin within a single valley, e.g. 1.75 eV of monolayer MoS<sub>2</sub> in the above discussions. We find that monolayer WS<sub>2</sub> has the largest spin-polarized current, which is from its large SOC splitting. Although SOC splitting of monolayer WSe<sub>2</sub> is also large (around 0.47 eV), its group velocity difference  $\Delta_{nm}^c$  is smaller than other TMDs, resulting in a smaller spin current. Finally, many-electron effects [62] may quantitatively change these single-particle results, such as pumping-photon energies listed in Table I. However, without breaking any essential symmetry of the above discussions, many-electron effects will not fundamentally

TABLE I. Symmetries of interband Comparison of spin and charge current conductivity of monolayer TMDs for linear and circular polarizations. We list the conductivity (in unit  $\mu A/V^2$ ) at the characteristic photon frequency which is marked in the parentheses. This photon energy is the one starting to pump both two spin electrons within a single valley, e.g. 1.75 eV for monolayer MoS<sub>2</sub>.

Materials	Linear polarization		Circular polarization	
	Spin current (injection)	Charge current (shift)	Spin current (shift)	Charge current (injection)
MoS <sub>2</sub> (1.75 eV)	398	1	2	10
MoSe <sub>2</sub> (1.50 eV)	514	4	5	26
WS <sub>2</sub> (1.70 eV)	556	2	3	8
WSe <sub>2</sub> (1.65 eV)	360	1	2	15

change our main conclusions of photocurrents.

Interestingly, we find that the polarization direction of light can switch the directions of both spin and charge currents. Figs. 3e and 3f show PSC and charge current under different polarization directions for photon energy at 1.75 eV, in which the  $x$ -direction of MoS<sub>2</sub> (Fig. 2a) is set to be 0 degrees. The cosine function relations are observed for both spin and charge currents in the same phase. Thus, we can increase/decrease and even turn off the spin and charge currents by controlling the light polarization. This is from the relations between photo-conductivities:  $\eta_{xxX}^L = -\eta_{yyx}^L$  and  $\sigma_{xxX}^L = -\sigma_{yyx}^L$  enforced by the three-fold rotational symmetry of monolayer TMDs.

*Spin and charge currents under circularly polarized light:* For circularly components of photocurrents, the imaginary part of optical oscillation strength contributes to photocurrent (Eqs. 4 and 5). In Fig. 4a, we have plotted the calculated  $Im(v_{mn}^x(k)v_{nm}^y(k))$  of monolayer MoS<sub>2</sub> near  $K$  and  $-K$  valleys excited by photons with an energy of 1.8 eV. Our first-principles simulation confirms that  $Im(v_{mn}^x(k)v_{nm}^y(k))$  has odd parity (anti-phase) in reciprocal space. As we discussed in Eqs. 4 and 5, the parity of  $Im(v_{mn}^x(k)v_{nm}^y(k))$  is odd while the real part of optical oscillation strength is even. Thus, the shift-current mechanism alternatively generates a spin current under circularly polarized light as shown in Fig. 4b, in which spin-up and spin-down currents are in opposite direction. On the contrary, charge current is generated by the injection-current mechanism, characterized as the circularly photogalvanic effect. Importantly, compare the amplitude of PSC and charge current in Figs. 4b and 4c, we find that the charge current is much stronger than spin current and the non-spin-polarized current is dominant in the circular polarization case. Table I also confirms

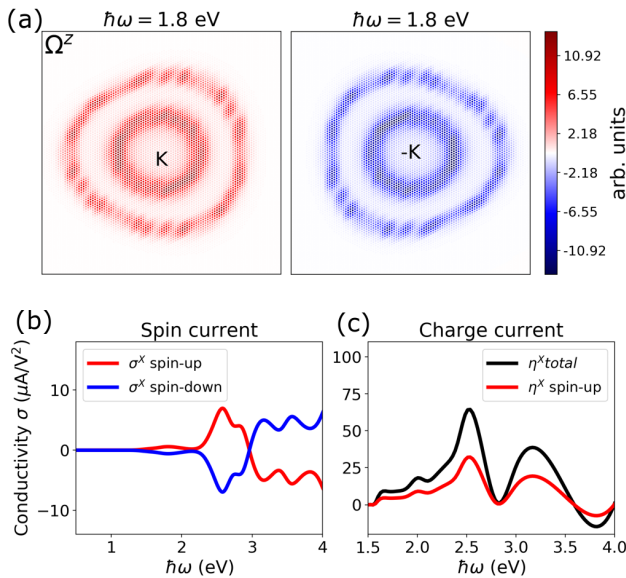


FIG. 4. Spin and charge currents under circular polarization: (a) Imaginary part of optical transition oscillations (similar to the Berry curvature) for  $\hbar\omega = 1.8$  eV photon excitation. (b) PSC and (c) charge current along the  $x$ -direction for circularly polarized light.

that the charge current is about an order of magnitude larger than the spin current in our calculated monolayer TMDs. Thus, we expect to observe the circularly photogalvanic effect in monolayer TMDs but with a weak spin polarization [39]. Similarly, the charge-current direction can be switched by the handedness of incident light.

Finally, our predicted spin photogalvanic effect is universal for noncentrosymmetric materials, including bulk GeTe, CdS, and 2D group IV monochalcogenides, and it does not depend on the origin of SOC. We noticed that the magnitude of circularly photogalvanic conductivity showed in Fig. 4c is one order smaller than that of PSC conductivity induced by linear polarized light. Thus, we expect that the PSC can be measured given the fact that the circularly photogalvanic effect is observed [45]. Our findings not only expand the understandings of nonlinear light-matter interaction physics but also substantially broadens our capability to manipulate spintronics in simple nonmagnetic crystals.

This work is supported by the National Science Foundation (NSF) CAREER grant No. DMR-1455346, and the Air Force Office of Scientific Research (AFOSR) grant No. FA9550-17-1-0304. The computational resources are provided by the Stampede of Teragrid at the Texas Advanced Computing Center (TACC) through XSEDE.

[1] I. Žutić, J. Fabian, and S. Das Sarma, *Rev. Mod. Phys.* **76**, 323 (2004).

[2] S. Bader and S. Parkin, *Annu. Rev. Condens. Matter Phys.* **1**, 71 (2010).

[3] S. Wolf, D. Awschalom, R. Buhrman, J. Daughton, v. S. von Molnár, M. Roukes, A. Y. Chtchelkanova, and D. Treger, *Science* **294**, 1488 (2001).

[4] C. H. Marrows and B. C. Dalton, *Physical Review Letters* **92**, 097206 (2004).

[5] R. R. Bhat, F. Nastos, A. Najmaie, and J. Sipe, *Physical Review Letters* **94**, 096603 (2005).

[6] V. E. Demidov, S. Urazhdin, H. Ulrichs, V. Tiberkevich, A. Slavin, D. Baither, G. Schmitz, and S. O. Demokritov, *Nature materials* **11**, 1028 (2012).

[7] T. Yang, T. Kimura, and Y. Otani, *Nature Physics* **4**, 851 (2008).

[8] D. D. Awschalom and M. E. Flatté, *Nature Physics* **3**, 153 (2007).

[9] R. Urban, G. Woltersdorf, and B. Heinrich, *Physical Review Letters* **87**, 217204 (2001).

[10] Y. Kajiwara, K. Harii, S. Takahashi, J.-i. Ohe, K. Uchida, M. Mizuguchi, H. Umezawa, H. Kawai, K. Ando, K. Takanashi, *et al.*, *Nature* **464**, 262 (2010).

[11] C. W. Sandweg, Y. Kajiwara, A. V. Chumak, A. A. Serga, V. I. Vasyuchka, M. B. Jungfleisch, E. Saitoh, and B. Hillebrands, *Physical Review Letters* **106**, 216601 (2011).

[12] A. Kimel, A. Kirilyuk, A. Tsvetkov, R. Pisarev, and T. Rasing, *Nature* **429**, 850 (2004).

[13] K. Uchida, S. Takahashi, K. Harii, J. Ieda, W. Koshibae, K. Ando, S. Maekawa, and E. Saitoh, *Nature* **455**, 778 (2008).

[14] C. Jaworski, J. Yang, S. Mack, D. Awschalom, J. Heremans, and R. Myers, *Nature Materials* **9**, 898 (2010).

[15] D. Qu, S. Huang, J. Hu, R. Wu, and C. Chien, *Physical Review Letters* **110**, 067206 (2013).

[16] S. Meyer, Y.-T. Chen, S. Wimmer, M. Althammer, T. Wimmer, R. Schlitz, S. Geprägs, H. Huebl, D. Ködderitzsch, H. Ebert, *et al.*, *Nature Materials* **16**, 977 (2017).

[17] P. Sheng, Y. Sakuraba, Y.-C. Lau, S. Takahashi, S. Mitani, and M. Hayashi, *Science Advances* **3**, e1701503 (2017).

[18] M. I. Dyakonov and V. Perel, *Physics Letters A* **35**, 459 (1971).

[19] J. Hirsch, *Physical Review Letters* **83**, 1834 (1999).

[20] Y. K. Kato, R. C. Myers, A. C. Gossard, and D. D. Awschalom, *Science* **306**, 1910 (2004).

[21] J. Wunderlich, B. Kaestner, J. Sinova, and T. Jungwirth, *Physical Review Letters* **94**, 047204 (2005).

[22] B. Huang, K.-H. Jin, B. Cui, F. Zhai, J. Mei, and F. Liu, *Nature Communications* **8**, 1 (2017).

[23] S. Murakami, N. Nagaosa, and S.-C. Zhang, *Science* **301**, 1348 (2003).

[24] J. Sinova, D. Culcer, Q. Niu, N. Sinitsyn, T. Jungwirth, and A. H. MacDonald, *Physical Review Letters* **92**, 126603 (2004).

[25] D. Xiao, G.-B. Liu, W. Feng, X. Xu, and W. Yao, *Physical Review Letters* **108**, 196802 (2012).

[26] S. D. Ganichev, E. L. Ivchenko, S. N. Danilov, J. Eroms, W. Wegscheider, D. Weiss, and W. Prettl, *Physical Review Letters* **86**, 4358 (2001).

[27] S. Ganichev, E. Ivchenko, V. Bel’Kov, S. Tarasenko, M. Sollinger, D. Weiss, W. Wegscheider, and W. Prettl, *Nature* **417**, 153 (2002).

[28] M. J. Stevens, A. L. Smirl, R. Bhat, A. Najmaie, J. Sipe,

- and H. Van Driel, *Physical Review Letters* **90**, 136603 (2003).
- [29] J. Hübner, W. Rühle, M. Klude, D. Hommel, R. Bhat, J. Sipe, and H. Van Driel, *Physical Review Letters* **90**, 216601 (2003).
- [30] D. Ellsworth, L. Lu, J. Lan, H. Chang, P. Li, Z. Wang, J. Hu, B. Johnson, Y. Bian, J. Xiao, *et al.*, *Nature Physics* **12**, 861 (2016).
- [31] R. von Baltz and W. Kraut, *Physical Review B* **23**, 5590 (1981).
- [32] S. M. Young, F. Zheng, and A. M. Rappe, *Physical review letters* **109**, 236601 (2012).
- [33] J. Sipe and A. Shkrebtii, *Physical Review B* **61**, 5337 (2000).
- [34] T. Morimoto, S. Zhong, J. Orenstein, and J. E. Moore, *Physical Review B* **94**, 245121 (2016).
- [35] F. de Juan, A. G. Grushin, T. Morimoto, and J. E. Moore, *Nature Communications* **8**, 1 (2017).
- [36] I. Sodemann and L. Fu, *Physical Review Letters* **115**, 216806 (2015).
- [37] Q. Ma, S.-Y. Xu, H. Shen, D. MacNeill, V. Fatemi, T.-R. Chang, A. M. M. Valdivia, S. Wu, Z. Du, C.-H. Hsu, *et al.*, *Nature* **565**, 337 (2019).
- [38] K. Kang, T. Li, E. Sohn, J. Shan, and K. F. Mak, *Nature Materials* **18**, 324 (2019).
- [39] D.-F. Shao, S.-H. Zhang, G. Gurung, W. Yang, and E. Y. Tsybmal, *Physical Review Letters* **124**, 067203 (2020).
- [40] H. Wang and X. Qian, *npj Computational Materials* **5**, 1 (2019).
- [41] S. Singh, J. Kim, K. M. Rabe, and D. Vanderbilt, *arXiv preprint arXiv:2001.08283* (2020).
- [42] “See Supplemental Material at xx, which includes Refs. [46-49]. We show derivations of both injection and shift current under linear and circular polarization using Feynman diagrams approach, the first-principles calculation details, and,”.
- [43] D. E. Parker, T. Morimoto, J. Orenstein, and J. E. Moore, *Phys. Rev. B* **99**, 045121 (2019).
- [44] D. Xiao, M.-C. Chang, and Q. Niu, *Reviews of Modern Physics* **82**, 1959 (2010).
- [45] H. Yuan, X. Wang, B. Lian, H. Zhang, X. Fang, B. Shen, G. Xu, Y. Xu, S.-C. Zhang, H. Y. Hwang, *et al.*, *Nature Nanotechnology* **9**, 851 (2014).
- [46] G. Kresse and J. Furthmüller, *Phys. Rev. B* **54**, 11169 (1996).
- [47] G. Kresse and D. Joubert, *Phys. Rev. B* **59**, 1758 (1999).
- [48] J. P. Perdew, K. Burke, and M. Ernzerhof, *Phys. Rev. Lett.* **77**, 3865 (1996).
- [49] P. Giannozzi, S. Baroni, N. Bonini, M. Calandra, R. Car, C. Cavazzoni, D. Ceresoli, G. L. Chiarotti, M. Cococcioni, I. Dabo, *et al.*, *Journal of physics: Condensed matter* **21**, 395502 (2009).
- [50] H. Zeng, J. Dai, W. Yao, D. Xiao, and X. Cui, *Nature Nanotechnology* **7**, 490 (2012).
- [51] T. Cao, G. Wang, W. Han, H. Ye, C. Zhu, J. Shi, Q. Niu, P. Tan, E. Wang, B. Liu, *et al.*, *Nature Communications* **3**, 1 (2012).
- [52] K. F. Mak, K. He, J. Shan, and T. F. Heinz, *Nature Nanotechnology* **7**, 494 (2012).
- [53] G.-B. Liu, W.-Y. Shan, Y. Yao, W. Yao, and D. Xiao, *Physical Review B* **88**, 085433 (2013).
- [54] Y. Saito, Y. Nakamura, M. S. Bahramy, Y. Kohama, J. Ye, Y. Kasahara, Y. Nakagawa, M. Onga, M. Tokunaga, T. Nojima, *et al.*, *Nature Physics* **12**, 144 (2016).
- [55] K. Hao, G. Moody, F. Wu, C. K. Dass, L. Xu, C.-H. Chen, L. Sun, M.-Y. Li, L.-J. Li, A. H. MacDonald, *et al.*, *Nature Physics* **12**, 677 (2016).
- [56] G. Wang, A. Chernikov, M. M. Glazov, T. F. Heinz, X. Marie, T. Amand, and B. Urbaszek, *Reviews of Modern Physics* **90**, 021001 (2018).
- [57] H. Wang, C. Zhang, W. Chan, S. Tiwari, and F. Rana, *Nature Communications* **6**, 1 (2015).
- [58] K. Kaasbjerg, K. S. Thygesen, and K. W. Jacobsen, *Phys. Rev. B* **85**, 115317 (2012).
- [59] B. Radisavljevic and A. Kis, *Nature Materials* **12**, 815 (2013).
- [60] Y. Song and H. Dery, *Phys. Rev. Lett.* **111**, 026601 (2013).
- [61] A. Dankert and S. P. Dash, *Nature Communications* **8**, 16093 (2017).
- [62] D. Y. Qiu, F. H. da Jornada, and S. G. Louie, *Phys. Rev. Lett.* **111**, 216805 (2013).

# Supplementary Information: Intrinsic Spin Photogalvanic Effect in Nonmagnetic Insulator

## INJECTION CURRENT MECHANISM

We adapt the Feynman diagram approach to calculate the injection current. Using the Feynman rules derived by D. E. Parker et.al.[1], we can easily calculate the corresponding injection-current tensors. Fig. S1 shows the Feynman diagrams of injection-current. Here, we use four diagrams to distinguish the order of polarization direction, and the conduction band  $m$  and valence band  $n$ .

For the one-photon pole under the velocity gauge, it contribute velocity matrix element  $\langle \alpha | \hat{v}_a | \beta \rangle$  for band  $\alpha$  translated to any band  $\beta$ . Here, in the above-discussed diagram, we have inter-band velocity matrix element  $\langle m | \hat{v}_a | n \rangle$  and intra-band velocity matrix element  $\langle n | \hat{v}_a | n \rangle$  and  $\langle m | \hat{v}_a | m \rangle$ . The occupation number of conduction and valence band is  $f_m = 0$  and  $f_n = 1$ , respectively.

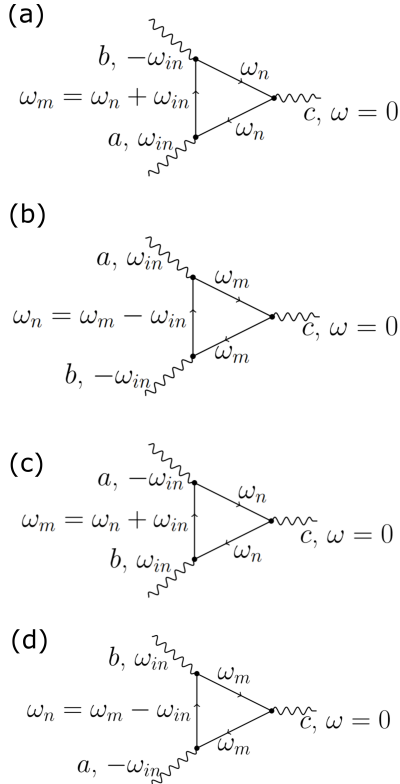


FIG. S1. The Feynman diagram for the injection current. The difference between the four diagrams are the different orders of polarized direction of light and the valence and conduction bands.

The first diagram shown by Fig. S1 (a) contribute to

$$\begin{aligned}
 \eta_1(0; \omega_{in}, -\omega_{in}) &= \frac{e^3}{\hbar^2 \omega_{in}^2} \sum_{mn} \int \frac{d^3k}{(2\pi)^3} \int d\omega' G_n(\omega') G_m(\omega' + \omega_{in}) G_n(\omega') \\
 &\quad \cdot \langle n | \hat{v}_a | m \rangle \langle m | \hat{v}_b | n \rangle \langle n | \hat{v}_c | n \rangle \\
 &= \frac{e^3}{\hbar^2 \omega_{in}^2} \sum_{mn} \int \frac{d^3k}{(2\pi)^3} \int d\omega' \frac{1}{\omega' - \omega_n + i\xi_n} \frac{1}{\omega' + \omega_{in} - \omega_m + i\xi_m} \\
 &\quad \cdot \frac{1}{\omega' - \omega_n + i\xi_n} \langle n | \hat{v}_a | m \rangle \langle m | \hat{v}_b | n \rangle \langle n | \hat{v}_c | n \rangle
 \end{aligned} \tag{S1}$$

where the  $G(\omega)$  is the free quasi-particle propagator with a dressed version.  $\xi$  is the imaginary part of the self-energy for the quasi-particle.

To evaluate the integrals such as

$$\begin{aligned}
 I(\omega_{in}, -\omega_{in}) &= \int d\omega' G_n(\omega') G_m(\omega' + \omega_{in}) G_n(\omega') \\
 &= \int d\omega' \frac{1}{\omega' - \omega_n + i\xi_n} \frac{1}{\omega' + \omega_{in} - \omega_m + i\xi_m} \frac{1}{\omega' - \omega_n}
 \end{aligned} \tag{S2}$$

We directly use the formalism deviated from the contour integral techniques with Matsubara frequencies [1].

$$\begin{aligned}
 I_3(\omega_{in}, -\omega_{in}) &= \frac{(-\omega_{in} - \omega_{nm})f_{nm} + (\omega_{in} - \omega_{mn})f_{nm}}{(\omega_{in} - \omega_{mn})(-\omega_{in} - \omega_{nm})(\omega - \omega_{nn} + i\xi)} \\
 &= \left( \frac{f_{nm}}{\omega_{in} - \omega_{mn}} + \frac{f_{nm}}{-\omega_{in} - \omega_{nm}} \right) \frac{1}{\omega - \omega_{nn} + i\xi} \\
 &= f_{nm} \left( \wp\left(\frac{1}{\omega_{in} - \omega_{mn}}\right) + \wp\left(\frac{1}{-\omega_{in} - \omega_{nm}}\right) \right. \\
 &\quad \left. + 2i\pi\delta(\omega_{in} - \omega_{mn}) \right) \cdot \frac{1}{\omega - \omega_{nn} + i\xi}
 \end{aligned} \tag{S3}$$

where the  $\wp\left(\frac{1}{\omega_{in} - \omega_{mn}}\right)$  is the principle part.  $f_{nm} = f_n - f_m$  where  $f_n$  and  $f_m$  are the occupation number. Because the principle part is odd while the  $\delta$  function is even, only imaginary part is non-vanishing. Thus, the first diagram contribution is

$$\begin{aligned}
 \eta_1(0; \omega_{in}, -\omega_{in}) &= \frac{2i\pi e^3}{\hbar^2 \omega_{in}^2} \sum_{mn} \int \frac{d^3k}{(2\pi)^3} \langle n | \hat{v}_a | m \rangle \langle m | \hat{v}_b | n \rangle \\
 &\quad \cdot \frac{\langle n | \hat{v}_c | n \rangle}{\omega - \omega_{nn} + i\xi} \delta(\omega_{in} - \omega_{mn})
 \end{aligned} \tag{S4}$$

Similarly, the contribution of the other three diagrams are

$$\begin{aligned} \eta_2(0; \omega_{in}, -\omega_{in}) &= \frac{2i\pi e^3}{\hbar^2 \omega_{in}^2} \sum_{mn} \int \frac{d^3k}{(2\pi)^3} f_{mn} \langle n|\hat{v}_a|m\rangle \langle m|\hat{v}_b|n\rangle \\ &\quad \cdot \frac{\langle m|\hat{v}_c|m\rangle}{\omega - \omega_{mm} + i\xi} \delta(\omega_{in} - \omega_{mn}) \end{aligned} \quad (S5)$$

$$\begin{aligned} \eta_3(0; \omega_{in}, -\omega_{in}) &= \frac{2i\pi e^3}{\hbar^2 \omega_{in}^2} \sum_{mn} \int \frac{d^3k}{(2\pi)^3} f_{nm} \langle n|\hat{v}_b|m\rangle \langle m|\hat{v}_a|n\rangle \\ &\quad \cdot \frac{\langle n|\hat{v}_c|n\rangle}{\omega - \omega_{nn} + i\xi} \delta(\omega_{in} - \omega_{mn}) \end{aligned} \quad (S6)$$

$$\begin{aligned} \eta_4(0; \omega_{in}, -\omega_{in}) &= \frac{2i\pi e^3}{\hbar^2 \omega_{in}^2} \sum_{mn} \int \frac{d^3k}{(2\pi)^3} f_{mn} \langle n|\hat{v}_b|m\rangle \langle m|\hat{v}_a|n\rangle \\ &\quad \cdot \frac{\langle m|\hat{v}_c|m\rangle}{\omega - \omega_{mm} + i\xi} \delta(\omega_{in} - \omega_{mn}) \end{aligned} \quad (S7)$$

### Linearly polarized light

For the linearly polarized light, the current density is  $j_c^L = \eta_c^L (E_a \cos(\theta) + E_b \sin(\theta))(E_a \cos(\theta) + E_b \sin(\theta)) = \eta_{aac}^L E_a^2 \cos^2(\theta) + \eta_{bbc}^L E_b^2 \sin^2(\theta) + (\eta_{abc}^L + \eta_{bac}^L) E_a E_b \cos(\theta) \sin(\theta)$ .

Here, we use the occupation number relation  $f_{vc} = -f_{cv} = f_v - f_c = 1$ . If we use the electron-hole symmetry within the relaxation time approximation. i.e.  $\tau_m = \tau_n = 1/\xi \equiv \tau$ . Then, the corresponding injection current conductivity tensors under linearly polarized light is

$$\begin{aligned} \eta_{abc}^L = \eta_{bac}^L &\equiv \frac{1}{4}(\eta_1 + \eta_2 + \eta_3 + \eta_4) = \\ &= \frac{\pi e^3}{2\hbar^2 \omega_{in}^2} \sum_{nm} \int \frac{d^3k}{(2\pi)^3} (\langle n|\hat{v}_a|m\rangle \langle m|\hat{v}_b|n\rangle + \langle n|\hat{v}_b|m\rangle \langle m|\hat{v}_a|n\rangle) \\ &\quad \cdot (\langle n|\hat{v}_c|n\rangle - \langle m|\hat{v}_c|m\rangle) \tau \delta(\omega_{in} - \omega_{mn}) \end{aligned} \quad (S8)$$

Specially, the diagonal component tensor of the injection current conductivity (e.g.  $a = b \equiv a$ ) is

$$\begin{aligned} \eta_{aac}^L &= \frac{\pi e^3}{\hbar^2 \omega_{in}^2} \sum_{mn} \int \frac{d^3k}{(2\pi)^3} |\langle n|\hat{v}_a|m\rangle|^2 (\langle n|\hat{v}_c|n\rangle - \langle m|\hat{v}_c|m\rangle) \\ &\quad \cdot \tau \delta(\omega_{in} - \omega_{mn}) \end{aligned} \quad (S9)$$

### Circularly polarized light

Next, we derive the circular component tensor of the injection current conductivity. For the time-reversal invariant non-centrosymmetric semiconductors, the injection current is non-vanishing under circular polarization. For right-hand circularly polarized light, the total current density  $j_c^\circ = \eta_c(E_a - iE_b)(E_a + iE_b) = \eta_{aac}^L E_a^2 + \eta_{bbc}^L E_b^2 + i\eta_{abc}^\circ E_a E_b$ . While for the left-hand circularly polarized light, the current density is  $j_c^\circ = \eta_c(E_a + iE_b)(E_a - iE_b) = \eta_{aac}^L E_a^2 + \eta_{bbc}^L E_b^2 + i\eta_{abc}^\circ E_a E_b$ . For the circular component of current conductivity tensor, we can get the relation  $\eta_{abc}^\circ = -\eta_{abc}^\circ$ .

we also use the occupation number relation  $f_{vc} = -f_{cv} = f_v - f_c = 1$ , and the electron-hole symmetry within the relaxation time approximation. i.e.  $\tau_c = \tau_v = 1/\xi$ . The the circular component tensor of the injection current conductivity is

$$\begin{aligned} \eta_{abc}^\circ = -\eta_{abc}^\circ &= \frac{1}{2}(\eta_1 + \eta_2 - \eta_3 - \eta_4) \\ &= \frac{-\pi e^3}{\hbar^2 \omega_{in}^2} \sum_{mn} \int \frac{d^3k}{(2\pi)^3} (\langle n|\hat{v}_a|m\rangle \langle m|\hat{v}_b|n\rangle - \langle n|\hat{v}_b|m\rangle \langle m|\hat{v}_a|n\rangle) \\ &\quad \cdot (\langle n|\hat{v}_c|n\rangle - \langle m|\hat{v}_c|m\rangle) \tau \delta(\omega_{in} - \omega_{mn}) \\ &= \frac{-2i\pi e^3}{\hbar^2 \omega_{in}^2} \sum_{mn} \int \frac{d^3k}{(2\pi)^3} Im(\langle n|\hat{v}_a|m\rangle \langle m|\hat{v}_b|n\rangle) \\ &\quad \cdot (\langle n|\hat{v}_c|n\rangle - \langle m|\hat{v}_c|m\rangle) \tau \delta(\omega_{in} - \omega_{mn}) \end{aligned} \quad (S10)$$

The Eq. S10 is same as the usually used formalism deviated by Sipe et. al. [2] based on the polarization operator method. We note that in Ref. [2], the injection current tensor  $2\eta_2^{abc}$  is equivalent to the  $\eta_{abc}^\circ$  in our case.

### SHIFT CURRENT MECHANISM

In the ab-initio framework, the precision achievable for the computation of nonlinear optical response is in general still poor when compared with the quality of calculated first-order optical properties. Here, we aim to construct the methodology of shift current nonlinear optical response tensor.



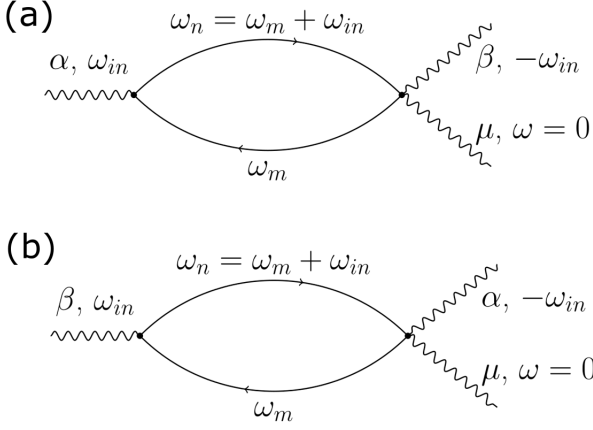


FIG. S2. The Feynman diagram for the shift current. The difference between the four diagrams are the different orders of polarized direction of light.

### Linearly polarized light

The shift current conductivity tensor at the single-particle approximation level (shown in Fig.S2) [1] is

$$\begin{aligned} & \sigma_{\alpha\beta\gamma}^L(0; \omega_{in}, -\omega_{in}) \\ &= \frac{e^3}{\hbar^2 \omega_{in}^2} \sum_{mn} \int \frac{d^3k}{(2\pi)^3} \int d\omega' G_m(\omega') G_n(\omega' + \omega_{in}) \\ & \quad \cdot (\langle m|\hat{v}_\alpha|n\rangle \langle n|\hat{v}_\beta|m\rangle_{;\mu} + \langle m|\hat{v}_\beta|n\rangle \langle n|\hat{v}_\alpha|m\rangle_{;\mu}) \end{aligned} \quad (\text{S11})$$

where  $\langle m|\hat{v}_\alpha|n\rangle$  is contributed by the one-photon vertex, and  $\langle n|\hat{v}_\alpha|m\rangle_{;\mu}$  is contributed by two-photon vertex using the velocity gauge. Here the  $\langle n|\hat{v}_\alpha|m\rangle_{;\mu}$  is defined as  $\frac{\partial \langle n|\hat{v}_\alpha|m\rangle}{\partial k_\mu} - i(A_{nn}^\mu - A_{mm}^\mu) \langle n|\hat{v}_\alpha|m\rangle$ , where  $A_n^\mu$  is the Berry connection. The  $\alpha$  and  $\beta$  are the polarized direction of light,  $\mu$  is the current direction. the  $G(\omega)$  is the free quasi-particle propagator with a dressed version, i.e.  $G_m(\omega') = \frac{1}{\omega' - \omega_m - i\xi}$ , where  $\omega_m$  is electron energy at mean-field theory,  $\xi$  is the imaginary part of quasi-particle energy.

To evaluate the integrals such as

$$\begin{aligned} I(\omega_{in}, -\omega_{in}) &= \int d\omega' G_m(\omega') G_n(\omega' + \omega_{in}) \\ &= \int d\omega' \frac{1}{\omega' - \omega_m} \cdot \frac{1}{\omega' + \omega_{in} - \omega_n} \end{aligned} \quad (\text{S12})$$

We use the formalism deviated from the contour integral techniques with Matsubara frequencies [3]

$$I(\omega_{in}, -\omega_{in}) = \frac{f_{mn}}{\omega_{in} - \omega_{mn} + i\xi} \quad (\text{S13})$$

where  $f_{mn} = f_m - f_n$  is the occupation number difference of quasi-particle states  $|m\rangle$  and  $|n\rangle$ . In general,  $I(\omega_{in}, -\omega_{in})$  have real and imaginary part, similar to the dielectric susceptibility.

However, the current susceptibility  $\sigma(0; \omega_{in}, -\omega_{in})$  is real and the imaginary part is zero. To see this, we replace the quasi-particle states  $|m\rangle$  and  $|n\rangle$  to the conduction particle  $|c\rangle$  and valence particle  $|v\rangle$ .

1). If  $|m\rangle = |c\rangle$  and  $|n\rangle = |v\rangle$ , we have  $\omega_{in} = \omega > 0$ ; with Eq. S13, the Eq. S21 goes to

$$\begin{aligned} & \sigma_1^L(0; \omega, -\omega) \\ &= \frac{e^3}{\hbar^2 \omega^2} \sum_{vc} \int \frac{d^3k}{(2\pi)^3} \frac{f_{cv}}{\omega - \omega_{cv} + i\xi} \\ & \quad \left( \langle c|\hat{v}_\alpha|v\rangle \langle v|\hat{v}_\beta|c\rangle_{;\mu} + \langle c|\hat{v}_\beta|v\rangle \langle v|\hat{v}_\alpha|c\rangle_{;\mu} \right) \\ &= \frac{e^3}{\hbar^2 \omega^2} \sum_{vc} \int \frac{d^3k}{(2\pi)^3} \frac{1}{\omega - \omega_{cv} + i\xi} \\ & \quad \left( \hat{v}_{cv}^\alpha(k) \hat{v}_{vc;\mu}^\beta(k) + \hat{v}_{cv}^\beta(k) \hat{v}_{vc;\mu}^\alpha(k) \right) \end{aligned} \quad (\text{S14})$$

2). If  $|m\rangle = |v\rangle$  and  $|n\rangle = |c\rangle$ , we have  $\omega_{in} = -\omega < 0$ . Then, the Eq.S21 goes to

$$\begin{aligned} & \sigma_2^L(0; -\omega, \omega) \\ &= \frac{e^3}{\hbar^2 \omega^2} \sum_{vc} \int \frac{d^3k}{(2\pi)^3} \frac{f_{vc}}{-\omega - \omega_{vc} + i\xi} \\ & \quad \left( \langle v|\hat{v}_\alpha|c\rangle \langle c|\hat{v}_\beta|v\rangle_{;\mu} + \langle v|\hat{v}_\beta|c\rangle \langle c|\hat{v}_\alpha|v\rangle_{;\mu} \right) \\ &= \frac{e^3}{\hbar^2 \omega^2} \sum_{vc} \int \frac{d^3k}{(2\pi)^3} \frac{1}{\omega_{in} + \omega_{vc} - i\xi} \\ & \quad \left( \hat{v}_{vc}^\alpha(k) \hat{v}_{cv;\mu}^\beta(k) + \hat{v}_{vc}^\beta(k) \hat{v}_{cv;\mu}^\alpha(k) \right) \end{aligned} \quad (\text{S15})$$

When the system have the time-reversal symmetry, we have the following relations:

$$\begin{aligned} \hat{v}_{vc}^\alpha(k) \frac{\partial \hat{v}_{cv}^\beta(k)}{\partial k_\mu} &= -\hat{v}_{cv}^\alpha(-k) \frac{\partial \hat{v}_{vc}^\beta(-k)}{\partial (-k_\mu)} \\ \hat{v}_{vc}^\alpha(k) \hat{v}_{cv}^\beta(k) &= \hat{v}_{cv}^\alpha(-k) \hat{v}_{vc}^\beta(-k) \\ i\hat{\xi}_{vv}^\mu(k) &= -i\hat{\xi}_{vv}^\mu(-k) \end{aligned} \quad (\text{S16})$$

Using Eq. S16 and definition of  $\hat{v}_{cv;\mu}^\beta(k)$ , the Eq. S15

can change to

$$\begin{aligned}
& \sigma_2^L(0; -\omega, \omega) \\
&= \frac{e^3}{\hbar^2 \omega^2} \sum_{vc} \int \frac{d^3 k}{(2\pi)^3} \frac{1}{\omega + \omega_{cv} - i\xi} \\
&\quad (-\hat{v}_{cv}^\alpha(-k) \hat{v}_{vc;\mu}^\beta(-k) - \hat{v}_{cv}^\beta(-k) \hat{v}_{vc;\mu}^\alpha(-k)) \\
&= \frac{e^3}{\hbar^2 \omega^2} \sum_{vc} \int \frac{d^3 k}{(2\pi)^3} \frac{-1}{\omega - \omega_{cv} - i\xi} \\
&\quad (\hat{v}_{cv}^\alpha(k) \hat{v}_{vc;\mu}^\beta(k) + \hat{v}_{cv}^\beta(k) \hat{v}_{vc;\mu}^\alpha(k))
\end{aligned} \tag{S17}$$

We sum the Eq. S14 and Eq. S17, then the shift current susceptibility or conductivity is

$$\begin{aligned}
\sigma_{\alpha\beta\gamma}^L(0; \omega, -\omega) &= \frac{1}{2} (\sigma_1^L(0; \omega, -\omega) + \sigma_2^L(0; -\omega, \omega)) \\
&= \frac{i\pi e^3}{\hbar^2 \omega^2} \sum_{vc} \int \frac{d^3 k}{(2\pi)^3} (\hat{v}_{cv}^\alpha(k) \hat{v}_{vc;\mu}^\beta(k) + \hat{v}_{cv}^\beta(k) \hat{v}_{vc;\mu}^\alpha(k)) \\
&\quad \cdot \delta(\omega - \omega_{cv})
\end{aligned} \tag{S18}$$

We know that the  $\hat{v}_{vc;\mu}^\alpha = \frac{\partial \langle v | \hat{v}_\alpha | c \rangle}{\partial k_\mu} - i(A_{vv}^\mu - A_{cc}^\mu) \langle v | \hat{v}_\alpha | c \rangle$ . Here we let  $\langle v | \hat{v}_\alpha | c \rangle = | \langle v | \hat{v}_\alpha | c \rangle | e^{i\phi_{vc}^\alpha}$ , then  $\hat{v}_{vc;\mu}^\alpha = \frac{\partial | \langle v | \hat{v}_\alpha | c \rangle |}{\partial k_\mu} e^{i\phi_{vc}^\alpha} + (i \frac{\partial \phi_{vc}^\alpha}{\partial k_\mu} - i(A_{vv}^\mu - A_{cc}^\mu)) \langle v | \hat{v}_\alpha | c \rangle$ , where the  $\frac{\partial | \langle v | \hat{v}_\alpha | c \rangle |}{\partial k_\mu} e^{i\phi_{vc}^\alpha}$  is odd in the reciprocal space. Thus, the the shift current conductivity is

$$\begin{aligned}
\sigma_{\alpha\beta\gamma}^L(0; \omega, -\omega) &= \frac{-\pi e^3}{\hbar^2 \omega^2} \sum_{vc} \int \frac{d^3 k}{(2\pi)^3} (\hat{v}_{cv}^\alpha(k) \hat{v}_{vc}^\beta(k) R_{vc}^{\alpha,\mu}(k) + \\
&\quad \hat{v}_{cv}^\beta(k) \hat{v}_{vc}^\alpha(k) R_{vc}^{\beta,\mu}(k)) \cdot \delta(\omega - \omega_{cv})
\end{aligned} \tag{S19}$$

where the shift vector  $R_{vc}^{\alpha,\mu}(k) = \frac{\partial \phi_{vc}^\alpha}{\partial k_\mu} - (A_{vv}^\mu - A_{cc}^\mu)$ . In the isotropic system, e.g. MoS<sub>2</sub>, the the phase of the interband velocity matrix is not direction dependent, i. e.  $\phi_{vc}^\alpha \simeq \phi_{vc}^\beta$ . So Eq. S19 can be simplified as

$$\begin{aligned}
\sigma^L(0; \omega, -\omega) &= \frac{1}{2} (\sigma_1^L(0; \omega, -\omega) + \sigma_2^L(0; -\omega, \omega)) \\
&= \frac{-\pi e^3}{\hbar^2 \omega^2} \sum_{vc} \int \frac{d^3 k}{(2\pi)^3} (\hat{v}_{cv}^\alpha(k) \hat{v}_{vc}^\beta(k) + \hat{v}_{cv}^\beta(k) \hat{v}_{vc}^\alpha(k)) \\
&\quad R_{vc}^\mu(k) \cdot \delta(\omega - \omega_{cv})
\end{aligned} \tag{S20}$$

## Circularly polarized light

For the circular component of the shift current conductivity tensor, the formula is replace Eq. S11 by

$$\begin{aligned}
\sigma_{\alpha\beta\gamma}^\circ(0; \omega_{in}, -\omega_{in}) &= -\sigma_{\alpha\beta\gamma}^\circ(0; \omega_{in}, -\omega_{in}) \\
&= \frac{e^3}{\hbar^2 \omega_{in}^2} \sum_{mn} \int \frac{d^3 k}{(2\pi)^3} \int d\omega' G_m(\omega') G_n(\omega' + \omega_{in}) \\
&\quad \cdot (\langle m | \hat{v}_\alpha | n \rangle \langle n | \hat{v}_\beta | m \rangle_{;\mu} - \langle m | \hat{v}_\beta | n \rangle \langle n | \hat{v}_\alpha | m \rangle_{;\mu})
\end{aligned} \tag{S21}$$

Proceeding the derivation similar to the Eq. S12-S19, the circular component of the shift current conductivity is

$$\begin{aligned}
\sigma_{\alpha\beta\gamma}^\circ(0; \omega, -\omega) &= -\sigma_{\alpha\beta\gamma}^\circ(0; \omega_{in}, -\omega_{in}) \\
&= \frac{-\pi e^3}{\hbar^2 \omega^2} \sum_{vc} \int \frac{d^3 k}{(2\pi)^3} (\hat{v}_{cv}^\alpha(k) \hat{v}_{vc}^\beta(k) - \hat{v}_{cv}^\beta(k) \hat{v}_{vc}^\alpha(k)) \\
&\quad R_{vc}^\mu(k) \cdot \delta(\omega - \omega_{cv})
\end{aligned} \tag{S22}$$

To consistent with the indices of injection current in our manuscript, we replace the band index c and v by m and n respectively, the directional index  $\alpha, \beta, \gamma$  by index a, b, c respectively.

## FIRST-PRINCIPLES COMPUTATIONAL DETAILS

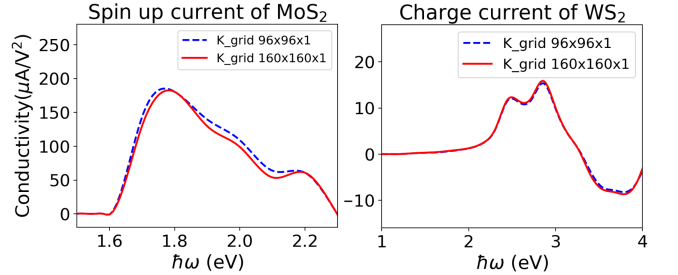


FIG. S3. (left) The spin up current conductivity  $\eta_{xx}^L$  of monolayer MoS<sub>2</sub> using  $96 \times 96 \times 1$  and  $160 \times 160 \times 1$  k-grid samples. (Right) The charge current conductivity  $\sigma_{xx}^L$  of monolayer MoS<sub>2</sub> using  $96 \times 96 \times 1$  and  $160 \times 160 \times 1$  k-grid samples.

The First principles calculations such as velocity matrix, optical oscillate strength, Berry curvature are mainly performed with the Vienna Ab-initio Simulation Package (VASP) [4] using the projector augmented wave method [5] and the plane-wave basis with an energy cutoff of 500 eV. The Perdew-Burke-Ernzerhof (PBE)

exchange-correlation functional [6] was used with spin-orbital coupling (SOC). The shift vector, and shift current conductivity are also checked using the Quantum ESPRESSO package[7] with PBE exchange-correlation functional.

The Structure optimizations were performed with a force criterion of  $0.01 \text{ eV}/\text{\AA}$ . The Monkhorst-Pack k-point meshes of  $10 \times 10 \times 1$  were adopted for the calculations of monolayer TMDs structures.

For nonlinear photocurrent calculation, we use the Monkhorst-Pack k-point meshes of  $160 \times 160 \times 1$  to get the converged spin and charge current. Fig. S3 presents the spin current conductivity element  $\eta_{xxX}^L$  of MoS<sub>2</sub> (left) and the charge current conductivity element  $\sigma_{xxX}^L$  of WS<sub>2</sub> (right) for different k-grid samples. The results using the k-point meshes of  $160 \times 160 \times 1$  are converged.

## INJECTION CURRENT CONTRIBUTIONS

### Spin current under linear polarization

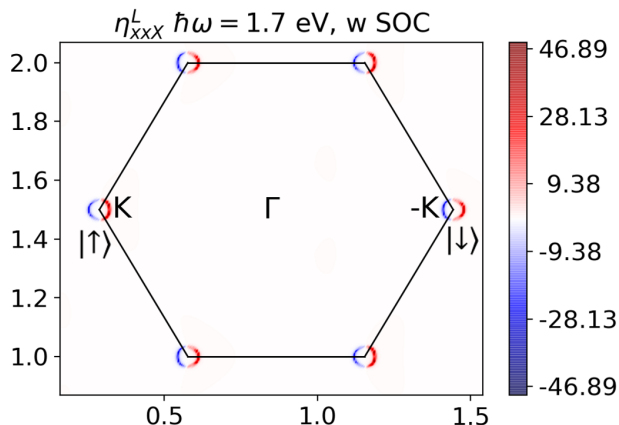


FIG. S4. The spin current conductivity distributed in the reciprocal space. The K valley relate to the spin-up carrier excitation, while the -K valley relate to the spin-down carrier excitation at photon  $E=1.7 \text{ eV}$ .

Fig.S4 shows the spin current conductivity  $\eta_{xxX}^L$  of monolayer MoS<sub>2</sub> distributed in the reciprocal space. We plot the conductivity excited by the photon at  $E = 1.7 \text{ eV}$ , which relates to only single spin excitation at each valley. We can clear see that the spin-down and spin-up carrier has the opposite sign, representing that the two

spins travel in opposite direction. All the other TMDs is similar to that of MoS<sub>2</sub>.

### Charge current under circular polarization

Fig.S5 shows the charge current conductivity  $\eta_{xyX}^C$  of monolayer MoS<sub>2</sub> distributed in the reciprocal space. We

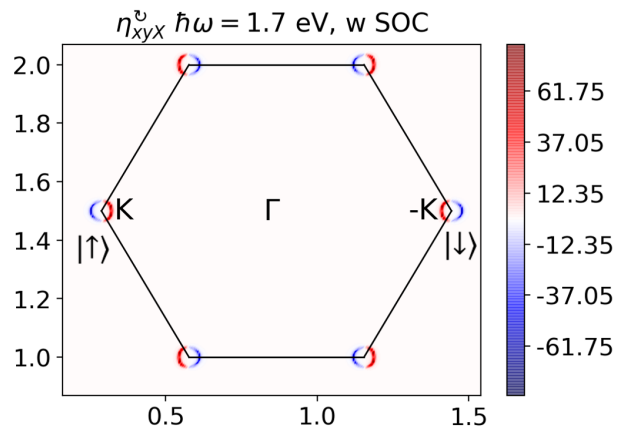


FIG. S5. The charge current conductivity distributed in the reciprocal space. The K valley relate to the spin-up carrier excitation, and the -K valley relate to the spin-down carrier excitation at photon  $E=1.7 \text{ eV}$ .

also plot the conductivity excited by the photon at  $E = 1.7 \text{ eV}$ . We note that the spin-down and spin-up carrier has the same sign, so the two spins travel in same direction.

- 
- [1] D. E. Parker, T. Morimoto, J. Orenstein, and J. E. Moore, Phys. Rev. B **99**, 045121 (2019).
  - [2] J. E. Sipe and A. I. Shkrebtii, Phys. Rev. B **61**, 5337 (2000).
  - [3] G. D. Mahan, *Many-particle physics* (Springer, Berlin, 2013).
  - [4] G. Kresse and J. Furthmüller, Phys. Rev. B **54**, 11169 (1996).
  - [5] G. Kresse and D. Joubert, Phys. Rev. B **59**, 1758 (1999).
  - [6] J. P. Perdew, K. Burke, and M. Ernzerhof, Phys. Rev. Lett. **77**, 3865 (1996).
  - [7] P. Giannozzi, S. Baroni, N. Bonini, M. Calandra, R. Car, C. Cavazzoni, D. Ceresoli, G. L. Chiarotti, M. Cococcioni, I. Dabo, *et al.*, Journal of physics: Condensed matter **21**, 395502 (2009).